PAPR Peak to average power ratio reduction techniques based on chirp selection for single and multi-user orthogonal chirp division multiplexing system

Vincent Savaux

PAPR Reduction Techniques Based on Chirp Selection for Single and Multi-User Orthogonal Chirp Division Multiplexing System

Vincent Savaux

Abstract

This paper deals with peak to average power (PAPR) reduction in a single and multi-user orthogonal chirp division multiplexing (OCDM) context. Two methods for PAPR reduction based on the selection of the frequency variation (up or down) of the chirps are first presented in a single user system. The first technique consists in considering two OCDM signals generated with up and down chirps, respectively, and selecting the one offering lowest PAPR. The second PAPR reduction method is based on usual clipping, and in that case the chirp selection aims to reduce the clipping noise. An adapted receiver is presented, based on the maximum likelihood (ML) estimation of the frequency variation (up or down) of the chirp. Then, a general procedure for multi-user OCDM transmission is introduced, where a sub-band of the available bandwidth is dedicated to each user, whose frequency of the chirps varies within this sub-band. Next, the PAPR reduction techniques are generalized to this multi-user OCDM system. Moreover, a performance analysis of the first PAPR reduction method is developed, and it is shown through simulations that theoretical and numerical results match for both Nyquist rate and oversampled signals. It is also shown that the chirp selection reduces the clipping noise, and improves the bit error rate (BER) performance compared with clipping only.

Index Terms

OCDM, PAPR, CCDF, Multicarrier, OFDM, Multi-user.

Manuscript submitted 2022

Vincent Savaux is with Institute of Research and Technology b<>com, Rennes, France (e-mails: vincent.savaux@b-com.com, Phone: +33 256 35 82 16.)

PAPR Reduction Techniques Based on Chirp Selection for Single and Multi-User Orthogonal Chirp Division Multiplexing System

I. Introduction

Orthogonal chirp division multiplexing (OCDM) is an emerging waveform which is based on Fresnel transform instead of Fourier transform in orthogonal frequency division multiplexing (OFDM) [1]. The main advantage of OCDM against OFDM or transform precoded OFDM, such as discrete Fourier transform-spread-OFDM (DFT-s-OFDM) used in 5G [2], lies in the fact that OCDM achieves an optimal decoding of the received signal in presence of time and frequency selective channels [3], whereas OFDM (resp. precoded OFDM) is only sub-optimal against frequency selective channel (resp. time selective channels) [4]. The optimality of OCDM is inherent to the use of chirps that spread the possible errors over the time and frequency grid. Furthermore, the use of chirps could be also relevant in the context of sensing and communications in 6G [5], since chirps are originally used in radar applications [6]. Another advantage inherent to OCDM is that it is backward compatible with OFDM-like waveforms used in numerous standards and technologies [7] such as WiFi, 4/5G, etc., as it has been shown in [7], [8] that the OCDM is equivalent to the OFDM modulation scheme, precoded with a DFT matrix and a multiplication by a chirp.

The high robustness against time and frequency selective channels is also a benefit of the the orthogonal time frequency space (OTFS) modulation [9] and the affine function division multiplexing (AFDM) [10], [11]. Although both waveforms can actually achieve "full diversity" against multipath mobile channels [10], unlike OCDM, they are not backward compatible with OFDM-like signals as they require dedicated transmitter and receiver structures, which may limit their deployment in practice. Otherwise, it has been shown that OCDM can also be used in optical communications [1], [12], [13] and underwater acoustic communications [14], [15]. Thus, the OCDM is an interesting candidate for a wide range of future communications systems. However, it has been noticed in [5] that some signal

processing techniques that are straightforward in OFDM need to be investigated in OCDM, such as multi-input multi-output (MIMO), peak to average power ratio (PAPR) reduction, or multi-user communication for instance. In fact, only few papers deal with these pending challenges to the date. In [16], the authors suggest an Alamouti space coding for MIMO-OCDM. The problem of PAPR reduction in OCDM is addressed in [17], [18], where usual methods are adapted from OFDM to OCDM.

In this paper, we tackle two topics of interest in the field of OCDM: PAPR reduction and multi-user OCDM. Thus, we suggest two techniques of PAPR reduction based on the selection of the frequency variation of the chirps (up or down chirps) at the transmitter. Two versions of the OCDM signal are generated at the transmitter side: one with up chirps and the other one with down chirps. The first method consists in selecting, on a symbol by symbol basis, the chirps that lead to the signal featuring the lowest PAPR. The second one consists in applying a clipping to both signals generated with up and down chirps, and the frequency variation of the transmitted chirps is chosen according to the minimum induced clipping noise. The proposed techniques are called OCDM with chirp selection (OCDM-CS) and clipping-driven driven chirp selection OCDM (OCDM-CDCS), respectively. In turn, we suggest a corresponding receiver where the variation of the chirp is estimated through a maximum likelihood (ML) estimator. Since they are based on the variation of the chirps, the proposed techniques are specific to OCDM, unlike those in [17], [18] where usual techniques are adapted from OFDM to OCDM.

As another original contribution, we introduce the multi-user OCDM system as a generalization of the system model introduced in [7], [8], [19], based on the fact that the precoded data subcarriers in the frequency domain are orthogonal. Thus, by applying a dedicated precoding process (DFT and multiplication by a chirp) to each user, the latter can be served by orthogonal signals. We then show that the suggested PAPR reduction methods can be generalized to multi-user OCDM systems, where a different frequency variation of chirps can be applied to each user. Alternatively, the principle can also be used for single user OCDM, where the data stream is split and mapped to different sub-bands, each sub-band being independently precoded, to the cost of an increase of the complexity of the system. In addition, the theoretical expression of the complementary cumulative distribution function (CCDF) of the PAPR is provided, and simulations results validate the analysis. Numerical results also show that OCDM-CS actually improves the PAPR, without bit error rate (BER) loss at the receiver. Moreover, OCDM-CDCS drastically reduces the PAPR (due to clipping),

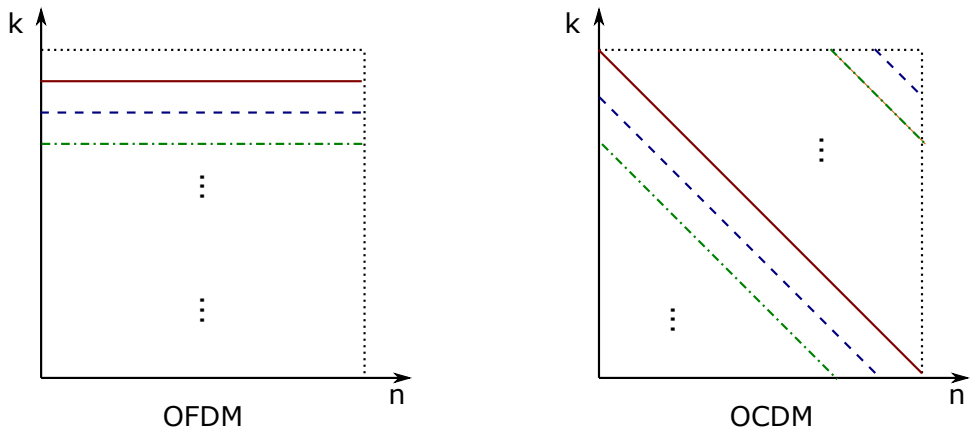

Fig. 1. Comparison of OFDM versus OCDM.

and allows to reduces the BER performance loss compared with the usual clipping thanks to the reduction of the clipping noise.

The rest of the paper is organized as follows: Section II introduces the DFT-based transmitter and receiver corresponding to the OCDM modulation and demodulation. Then the two suggested PAPR reduction methods based on chirps selection are presented in Section III. The corresponding adapted receiver including the ML estimator of the frequency variation of the chirps is detailed in Section IV, and the generalization of the techniques to multi-user OCDM is described in Section V. A PAPR performance analysis is developed in Section VI, and Section VII presents the simulations results. Finally, Section VIII concludes this paper.

Notations: $arg(.)$ is the argument (phase) operator, $Re\{.\}$ and $Im\{.\}$ indicate the real and the imaginary parts, respectively. $sign(a)$ returns the sign of a real a, the probability of an event A is denoted by $\mathbb{P}(A)$, and the mathematical expectation is written $\mathbb{E}\{.\}$. The convolution product is written as $(.*.)$.

II. Problem Statement

Any multicarrier signal x_n, $n = 0, 1, .., N-1$, can be generally expressed, when sampled at Nyquist rate (*i.e.* when the signal length N in time is equal to the number of subcarriers), as follows:

$$x_n = \frac{1}{N} \sum_{k=0}^{N-1} C_k g_{k,n}, \tag{1}$$

where k is the frequency index, $g_{k,n}$ is a given modulation filter depending on the waveform (the term *filter* is usually used in the field of signal processing applied to multicarrier signal),

and C_k is a symbol of constellation that we assume to be normalized, *i.e.* $\mathbb{E}\{|C_k|^2\} = 1$. Thus, in OFDM the filter is taken from the Fourier basis as

$$g^f_{k,n} = \exp\Big(2j\pi\frac{kn}{N}\Big), \tag{2}$$

where the superscript f refers to OFDM. In OCDM, the filter is based on chirp and can be expressed using the Fresnel transform basis, in the case where N is even, as

$$g^c_{k,n} = \exp\Big(-j\frac{\pi}{N}(n-k)^2 + j\frac{\pi}{4}\Big), \tag{3}$$

where the superscript c refers to OCDM. In the case where N is odd, the term $(n-k)$ in (3) is substituted by $(n-k+\frac{1}{2})$. In the rest of the paper, we assume that N is even for a sake of brevity, but all the developments and results hold for N odd as well. Fig. 1 illustrates the basic principle of OFDM and OCDM: in OFDM, $g^f_{k,n}$ has a constant frequency, whereas in OCDM, the instantaneous frequency of chirps linearly varies in time. In fact, it can be noticed from (2) and (3) that the phases of the filters in OFDM vary linearly, whereas they vary quadratically in OCDM. A thorough analysis in [1] shows that (1) using (3) corresponds to an inverse discrete Fresnel transform (IDFnT) of C_k, and can be simplified to a processing involving a simple inverse discrete Fourier transform (IDFT), to the cost of multiplications by quadratic phases in both the frequency and the time domains. It results that (1) using (3) can be rewritten as

$$x_n = \frac{e^{j\frac{\pi}{4}}}{N}\Big[\sum_{k=0}^{N-1} C_k e^{-j\pi\frac{k^2}{N}} e^{2j\pi\frac{kn}{N}}\Big] e^{-j\pi\frac{n^2}{N}}. \tag{4}$$

Alternatively in [8], the authors suggest to decompose the Fresnel transform into three main steps, such as illustrated in Fig. 2-(a):

1) a DFT of size K of the vector containing C_k,
2) the multiplication by the chirp $e^{-j\pi\frac{k^2}{N}}$,
3) an IDFT of size N, where N can be larger than the number of useful subcarriers K.

The advantage of the OCDM modulation scheme in [8] is that the sample rate at the output of the IDFT can be set larger than Nyquist rate, whereas the solution in (4) is limited to Nyquist rate. Moreover, it is proved in [8] that the orthogonality between chirps holds. We hereby mathematically formalize the principle of the OCDM modulation in [8]. First, it has been noticed in [20] that the DFT of a chirp $g_{k,n}$ is also a chirp in the frequency domain. Thus, by using the generalized quadratic Gauss sum [21], we have

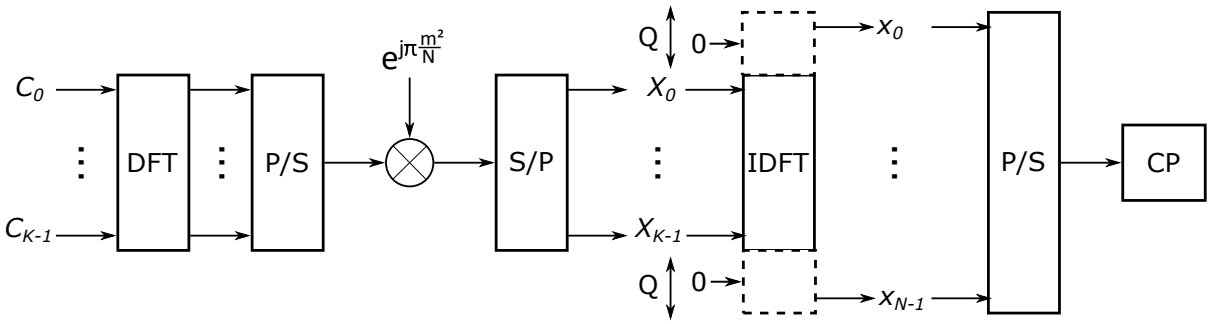

(a) DFT-based OCDM modulation.

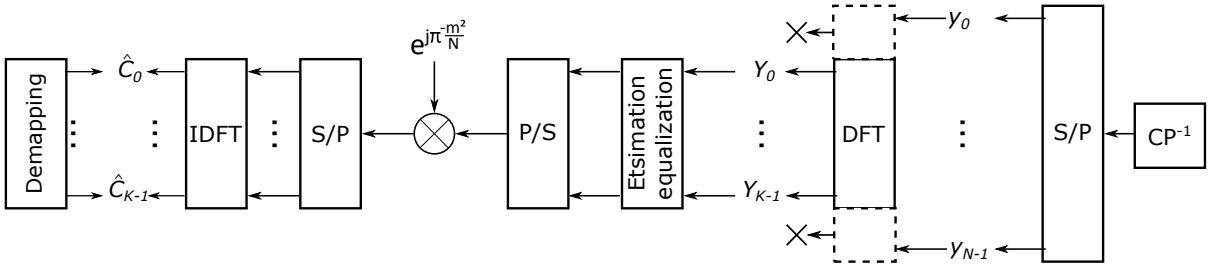

(b) DFT-based OCDM reception chain.

Fig. 2. DFT-based OCDM modulation (a) such as suggested in [8], and the corresponding reception chain (b).

$$\begin{aligned} G_{k,m} &= \sum_{n=0}^{N-1} g_{k,n} e^{-2j\pi \frac{mn}{N}} \\ &= e^{j\frac{\pi}{4}} \sum_{n=0}^{N-1} e^{\frac{j\pi}{N}(-n^2-k^2+2n(k-m))} \\ &= \sqrt{N} e^{j\frac{\pi}{N}(m^2-2km)}, \end{aligned} \tag{5}$$

where m is the index of the frequency sample. Then, by substituting $g_{k,n}$ in (1) by the IDFT of $G_{k,m}$, we obtain:

$$\begin{aligned} x_n &= \frac{1}{N} \sum_{k=0}^{N-1} C_k \Big[\frac{1}{N} \sum_{m=0}^{N-1} G_{k,m} e^{2j\pi \frac{mn}{N}} \Big] \\ &= \frac{\sqrt{N}}{N^2} \sum_{m=0}^{N-1} \Big[\sum_{k=0}^{N-1} C_k e^{j\frac{\pi}{N}(m^2-2km)} \Big] e^{2j\pi \frac{mn}{N}}. \end{aligned} \tag{6}$$

We can generalize (6) to consider a DFT of size $K \leq N$ corresponding to K symbols of data $\{C_0, C_1, .., C_{K-1}\}$ and a IDFT of size N. In that case $Q = \frac{N-K}{2}$ null subcarriers are located at the edge of the band such as illustrated in Fig. 2-(a). Then x_n is expressed as

$$x_n = \frac{\sqrt{K}}{KN} \sum_{m=0}^{N-1} \alpha_m \underbrace{e^{j\pi \frac{(m-Q)^2}{K}} \left[\sum_{k=0}^{K-1} C_k e^{-2j\pi \frac{k(m-Q)}{K}} \right]}_{X_m} e^{2j\pi \frac{mn}{N}}, \tag{7}$$

with $\alpha_m = 0$ if the m-th subcarrier is null, and $\alpha_m = 1$ otherwise. In addition, Fig. 2-(b) shows the OCDM reception chain, including the channel estimation and equalization. This topic is out of the scope of this paper, but details about channel estimation and equalization in OCDM can be found in [1], [4], [8]. Moreover, the remaining of the OCDM reception chain consists of the reverse unitary blocks corresponding to those at the transmitter, namely: the CP removal, the DFT (where null subcarrier can be removed), the multiplication by the inverse chirp, and the IDFT.

It has been shown in [17], [22] that OCDM, similarly to any multicarrier system that can be generally expressed as in (1), is prone to large PAPR since the samples of the signal x_n can be considered as complex Gaussian variables. It results that the complementary cumulative distribution function $CCDF$ of the the OCDM signal is the same as that of OFDM and can be expressed at Nyquist rate ($K = N$) as (see [23], [24])

$$\begin{aligned} CCDF(\lambda) =& \mathbb{P}\left(\frac{\max_n |x_n|^2}{\mathbb{E}\{|x_n|^2\}} \geq \lambda \right) \\ =& 1 - (1 - e^{-\lambda})^N, \end{aligned} \tag{8}$$

where $\frac{\max_n |x_n|^2}{\mathbb{E}\{|x_n|^2\}}$ is the expression of the PAPR. Moreover, we assume that $\mathbb{E}\{|x_n|^2\} = \frac{1}{N} \sum_{n=0}^{N-1} |x_n|^2$ and (8) hold for sufficiently large $N \geq 128$, otherwise see [25] for PAPR expressions considering lower N values. For largely oversampled signal, [23] proposed to generalize (8) as $CCDF(\lambda) = 1 - (1 - e^{-\lambda})^{\alpha.N}$ where α is empirically set to $\alpha = 2.8$. However, few methods for PAPR reduction in OCDM have been suggested in the literature [17], [18]. Furthermore, the authors of [17], [18] adapt existing methods such as clipping and selected mapping in [17], or tone reservation in [18]. We first introduce techniques of PAPR reduction dedicated to OCDM in Section III, then we present a generalization of the single-user OCDM transmission chain in Fig. 2 to multi-user OCDM and how the PAPR reduction techniques can be adapted to multi-user OCDM in Section V.

III. PAPR Reduction Methods Based on Chirp Selection

In this section, we present two methods of PAPR reduction for OCDM, based on the selection of the variation of the chirp (up or down). The techniques of PAPR reduction,

as well as the corresponding adapted receiver, are presented in a single user context, and generalized to multi-user OCDM afterward.

A. PAPR Driven Chirp Selection

It can be noticed in (6)-(7) or in Fig. 2 that the multiplication by the chirp $e^{j\pi\frac{m^2}{N}}$ leads to a sum of down chirps such as illustrated in the right side of Fig. 1. However, it is also mathematically possible to consider a multiplication by $e^{-j\pi\frac{m^2}{N}}$ instead of $e^{j\pi\frac{m^2}{N}}$ therefore leading to a sum of up chirps in (1). We define $\epsilon \in \{-1, 1\}$ such that the multiplication by $e^{j\epsilon\pi\frac{m^2}{N}}$ in (6)-(7) leads to $x_n^{(1)}$ (resp. $x_n^{(-1)}$) if $\epsilon = 1$ (resp. $\epsilon = -1$), and which are given by:

$$\begin{aligned} x_n^{(1)} =& \frac{1}{N}\sum_{k=0}^{N-1} C_k \underbrace{\exp\Big(-j\frac{\pi}{N}(n-k)^2 + j\frac{\pi}{4}\Big)}_{g_{k,n}^{(1)}}, \\ x_n^{(-1)} =& \frac{1}{N}\sum_{k=0}^{N-1} C_k \underbrace{exp\Big(j\frac{\pi}{N}(n-k)^2 - j\frac{\pi}{4}\Big)}_{g_{k,n}^{(-1)}}. \end{aligned} \tag{9}$$

Based on (9), the suggested PAPR reduction method called OCDM with chirp selection (OCDM-CS) consists in choosing at the transmitter side the signal $x_n^{(1)}$ or $x_n^{(-1)}$, $n = 0, 1, .., N-1$, offering the lowest PAPR, such as illustrated in Fig. 3. The values $PAPR^{(1)}$ and $PAPR^{(-1)}$ correspond to the PAPR of the signals $x_n^{(1)}$ and $x_n^{(-1)}$, respectively. The different steps of the method are detailed in Algorithm 1, where the inputs $x_n^{(1)}$ and $x_n^{(-1)}$ are obtained from any OCDM modulation method.

Algorithm 1: PAPR reduction method by chirp selection.

input : $(x_n^{(1)}, x_n^{(-1)})$

output: $x_n = x_n^{(1)}$ or $x_n = x_n^{(-1)}$

$PAPR^{(1)} \leftarrow \frac{\max_n |x_n^{(1)}|^2}{\mathbb{E}\{|x_n^{(1)}|^2\}}$

$PAPR^{(-1)} \leftarrow \frac{\max_n |x_n^{(-1)}|^2}{\mathbb{E}\{|x_n^{(-1)}|^2\}}$

if $PAPR^{(1)} > PAPR^{(-1)}$ **then**

  $x_n \leftarrow x_n^{(-1)}$

else

  $x_n \leftarrow x_n^{(1)}$

The advantages of the suggested algorithm are multiple:

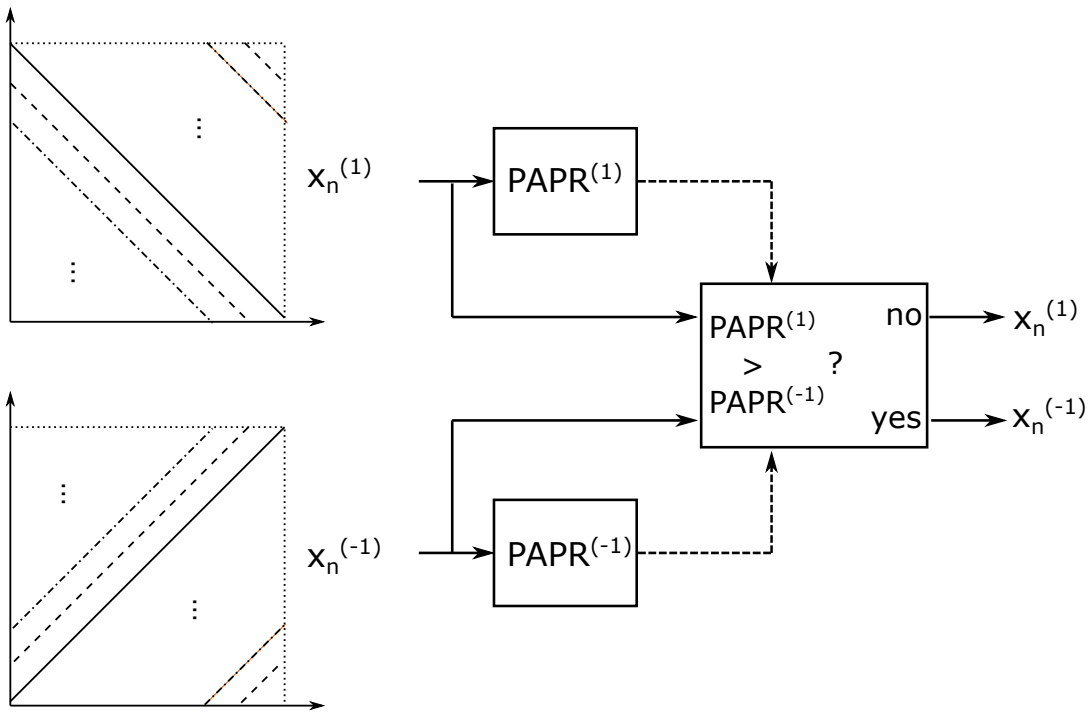

Fig. 3. Basic principle of the suggested PAPR reduction method by chirp selection, OCDM-CS.

- the method is simple to implement as it only requires a simple comparison between $PAPR^{(1)}$ and $PAPR^{(-1)}$,
- it is not destructive for the transmitted signal compared with clipping method [26] for instance,
- it can be associated with other techniques of reduction of PAPR [17], [18].

It is worth noticing that the suggested OCDM-CS method is very close to the so-called selected mapping (SLM) [17], where the data symbols C_k are multiplied by different phase sequences, and the sequence leading to the lowest PAPR is actually transmitted. In the OCDM-CS technique, the "phase sequence" is based on the variation of the chirp and applied to the DFT-encoded symbols. However, it can be expected that the OCDM-CS and the SLM (using two phase sequences) achieve the same performance.

B. Clipping Driven Chirp Selection

1) Clipping Method: The basic principle of the clipping method (when applied in its simplest implementation) is to clip any sample x_n that saturates, *i.e.* whose module $|x_n|$ (or equivalently $|x_n|^2$) exceeds a given threshold μ [27].In the following, we note with a superscript (c) the clipped samples as $x_n^{(c)}$. The value of μ can be chosen according to

different metrics: a target PAPR, a target error vector magnitude (EVM), a target probability of clipping P_t, etc. In the following, we consider the latter metric, which leads to:

$$\begin{aligned} P_t &= \mathbb{P}\Big(\frac{|x_n|^2}{\mathbb{E}\{|x_n|^2\}} \geq \mu\Big) \\ &= e^{-\mu} \\ \Leftrightarrow \mu &= -\ln(P_t), \end{aligned} \tag{10}$$

where $\frac{|x_n|^2}{\mathbb{E}\{|x_n|^2\}}$ is the square modulus of the normalized signal.

The main drawback of clipping is to induce non-linear distortions, which can be modeled as an additional white Gaussian noise [26]. The method hereby presented aims at reducing the induced clipping noise, by choosing among up and down chirps.

2) Description of the Method: Once again, based on (9), the suggested PAPR reduction method called OCDM with clipping-driven chirp selection (OCDM-CDCS) consists in choosing at the transmitter side the signal $x_n^{(1)}$ or $x_n^{(-1)}$ offering the lowest clipping noise for a given threshold value μ, such as illustrated in Fig. 4. The values $\sigma_c^2(1)$ and $\sigma_c^2(-1)$ correspond to the variances of the clipping noise of the clipped signals $x_n^{(1)}$ and $x_n^{(-1)}$, respectively. The different steps of the method are detailed as follows:

1) For any $n = 0, 1, .., N-1$, generate $x_n^{(1)}$ and $x_n^{(-1)}$ such as defined in (9) and normalize their power.
2) Clip $x_n^{(1)}$ and $x_n^{(-1)}$ to get $x_n^{(1,c)}$ and $x_n^{(-1,c)}$ such as described in Section III-B1.
3) Calculate the variances of the clipping noises. For any $\epsilon = \pm 1$, the variance of the clipping noise $\sigma_c^2(\epsilon)$ is given by

$$\sigma_c^2(\epsilon) = \frac{1}{N}\sum_{n=0}^{N-1} |x_n^{(\epsilon)} - x_n^{(\epsilon,c)}|^2. \tag{11}$$

4) If $\sigma_c^2(-1) > \sigma_c^2(1)$ transmit $x_n^{(1,c)}$, else transmit $x_n^{(-1,c)}$.

Both presented techniques lead to a PAPR reduction, such as shown in Section VII and are based on chirp selection, which is dedicated to the OCDM modulation. However, the two proposed techniques require two OCDM modulation chains in parallel (at least parts of modulation chains), which increases the computation cost at the transmitter side. Moreover, it requires an adapted receiver to discriminate up chirps or down chirp. A (sub-)optimal receiver based on the maximum likelihood criterion is hereby presented.

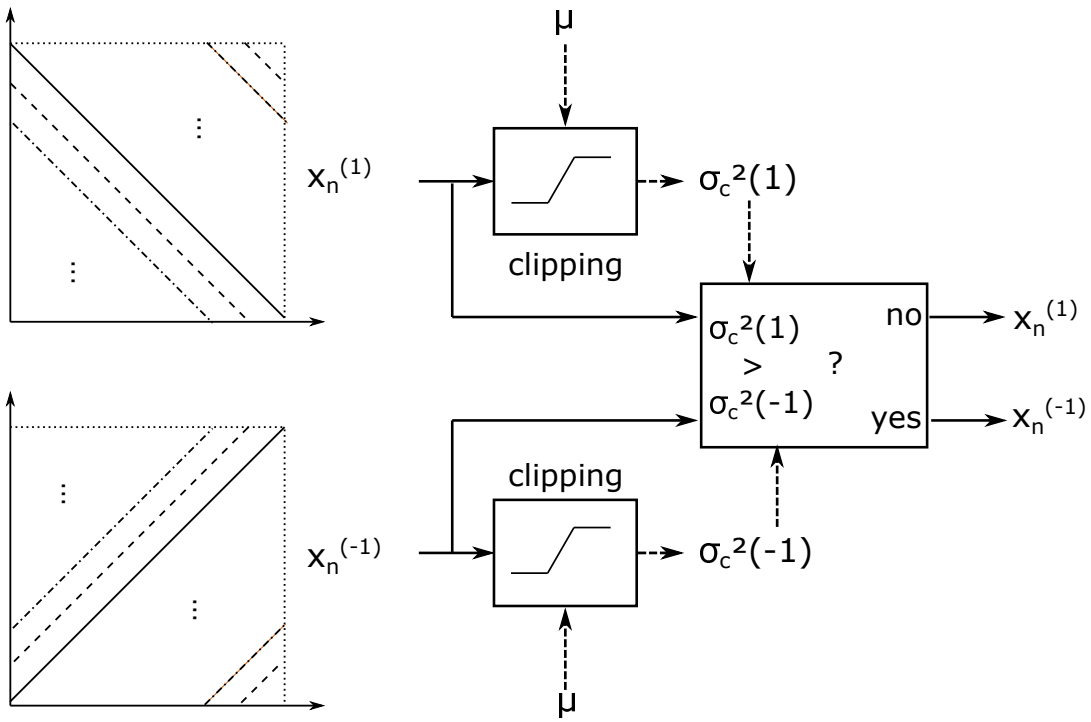

Fig. 4. Basic principle of the suggested PAPR reduction method based on clipping and chirp selection.

IV. Corresponding Adapted Receiver

The received OCDM signal samples y_n, $n = 0, 1, .., N-1$, assuming a coherent demodulation (*i.e.* after synchronization) and after CP removal, can be generally expressed as

$$y_n = (h * x^{(\epsilon)})_n + w_n, \tag{12}$$

where $\mathbf{h} = [h_0, h_1, .., h_{L-1}]$ is the vector of size $1 \times L$ containing the impulse response of the channel, where we assume that L is smaller than the CP, avoiding intersymbol interference. Moreover, $w_n \sim \mathbb{CN}(0, \sigma^2)$, $n = 0, 1, .., N-1$, are the samples of the complex additive white Gaussian noise (AWGN). Different receivers including an equalization stage have been suggested in the literature [1], [22], [28], according to the method of modulation (discrete Fresnel transform (1), IDFT (4), precoding and IDFT (6)-(7)). We hereby consider a DFT based receiver similar to the transmitter.

After the CP removal, the convolution in (12) becomes cyclic, therefore the DFT of size N of y_n, yields the frequency samples Y_m:

$$Y_m = H_m X_m^{(\epsilon)} + W_m, \tag{13}$$

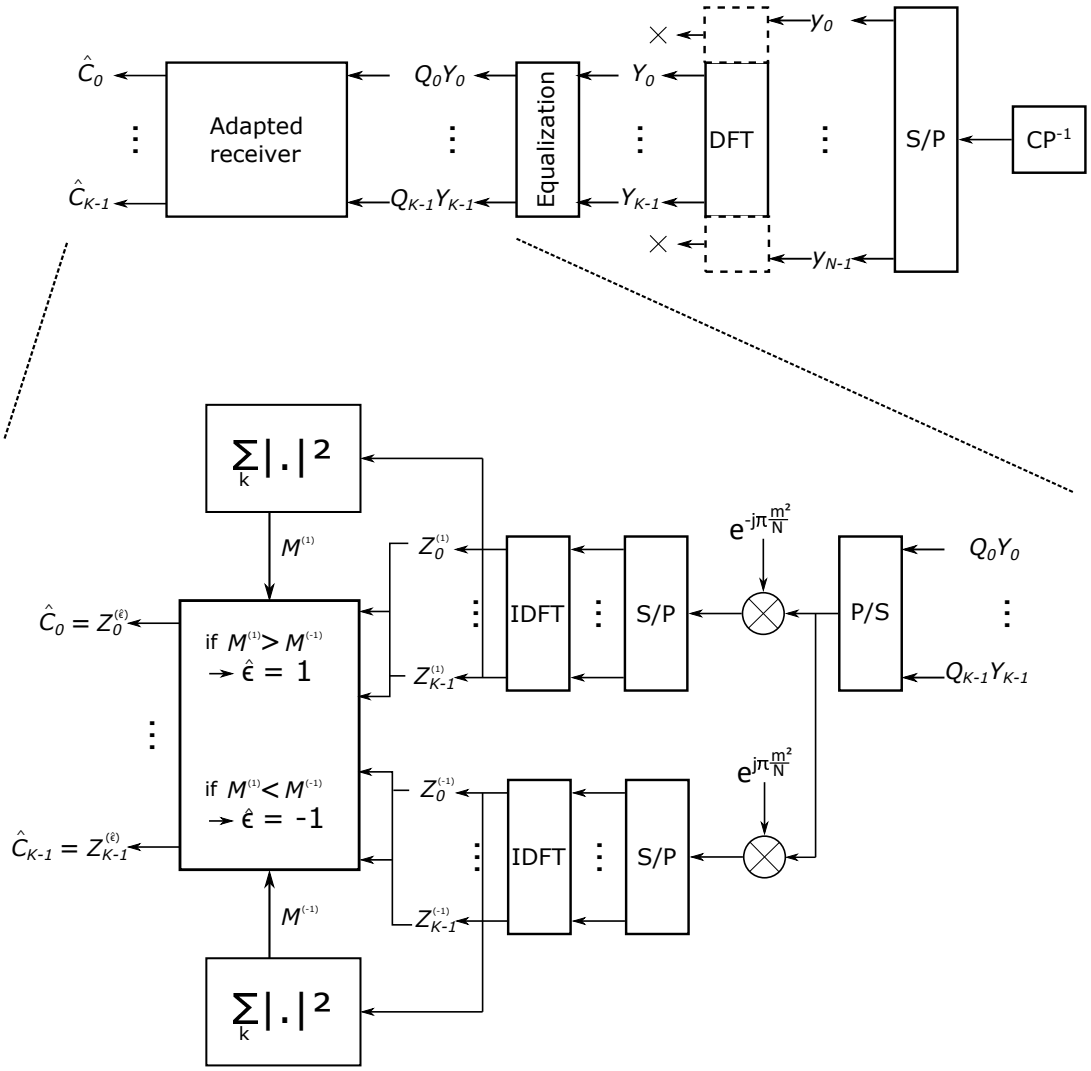

Fig. 5. OCDM receiver adapted to the PAPR reduction method based on chirp selection.

where $m = 0, 1, .., K-1$ after the null subcarrier removal, and H_m is the frequency response of the channel. The principle of the adapted receiver consists in estimating the variation of the chirps (up or down) from the observation Y_m, in order to properly demodulate the information symbols C_k. Thus, the estimation of down or up chirps reduces to the estimation of ϵ. The optimal estimator consists in maximizing the likelihood function as

$$\hat{\epsilon} = \underset{\epsilon \in \{-1,1\}}{\arg\max}\ C \exp\left(-\frac{1}{\sigma^2} \sum_{m=0}^{K-1} |Y_m - H_m X_m^{(\epsilon)}|^2 \right), \tag{14}$$

where $X_m^{(\epsilon)}$ corresponds to the samples obtained with $\epsilon = 1$ or $\epsilon = -1$, and C is a constant that does not needs to be defined as it will be removed from the following developments.

After some mathematical simplifications, (14) yields:

$$\begin{aligned}\hat{\epsilon} &= \underset{\epsilon\in\{-1,1\}}{\arg\max}\ C\exp\left(-\frac{1}{\sigma^2}\sum_{m=0}^{K-1}|Y_m|^2\right)\exp\left(-\frac{1}{\sigma^2}\sum_{m=0}^{K-1}|H_m X_m^{(\epsilon)}|^2\right)\\ &\qquad\times\exp\left(\frac{1}{\sigma^2}\sum_{m=0}^{K-1}2Re\Big\{Y_m H_m^*(X_m^{(\epsilon)})^*\Big\}\right)\\ &= \underset{\epsilon\in\{-1,1\}}{\arg\max}\ \sum_{m=0}^{K-1}Re\Big\{Y_m H_m^*(X_m^{(\epsilon)})^*\Big\},\end{aligned} \tag{15}$$

since the maximization is independent of Y_m and we assume that $\sum_{m=0}^{K-1}|H_m X_m^{(\epsilon)}|^2$ is independent of ϵ. The latter assumption is justified as the frequency samples $X_m^{(\epsilon)}$ are similar to zero mean Gaussian noise samples whose mean square is independent of ϵ. Then by substituting $X_m^{(\epsilon)}$ by its definition, we obtain:

$$\begin{aligned}\hat{\epsilon} &= \underset{\epsilon\in\{-1,1\}}{\arg\max}\ \sum_{m=0}^{K-1}Re\Big\{Y_m H_m^*\sum_{k=0}^{K-1}e^{-j\epsilon\pi\frac{m^2}{K}}C_k^* e^{2j\pi\frac{mk}{K}}\Big\}\\ &= \underset{\epsilon\in\{-1,1\}}{\arg\max}\ Re\Big\{\sum_{k=0}^{K-1}C_k^*\sum_{m=0}^{K-1}Y_m H_m^* e^{-j\epsilon\pi\frac{m^2}{K}}e^{2j\pi\frac{mk}{K}}\Big\},\end{aligned} \tag{16}$$

where we recognize the IDFT of $Y_m H_m^* e^{-j\epsilon\pi\frac{m^2}{K}}$. It is worth emphasizing that both H_m and C_k are unknown. To circumvent the lack of knowledge of H_m, it is possible to substitute $Y_m H_m^*$ by $Y_m Q_m$, where Q_m is the coefficient of a one-tap equalizer, *e.g.* zero forcing (ZF) or minimum mean square error (MMSE). In that case, the estimate $\hat{H}_m$ can be considered instead of H_m, e.g. for ZF equalizer $Q_m = \hat{H}_m^{-1}$. Note that, such as aforementioned, channel estimation in OCDM is out of the scope of this paper but some methods have been proposed in [19], [29]–[32]. However in the following, we will consider perfect channel estimation. On the other hand, C_k cannot be substituted, therefore we suggest a sub-optimal estimator of ϵ as follows:

$$\hat{\epsilon} = \underset{\epsilon\in\{-1,1\}}{\arg\max}\ \sum_{k=0}^{K-1}|Z_k^{(\epsilon)}|^2, \tag{17}$$

where we denoted $Z_k^{(\epsilon)} = \sum_{m=0}^{K-1}Y_m Q_m e^{-j\epsilon\pi\frac{m^2}{K}}e^{2j\pi\frac{mk}{K}}$ for clarity purpose. In fact, in ideal condition where $H_m = 1$, in absence of noise, and if ϵ is known, it can be observed that $Z_k^{(\epsilon)} = C_k$, and hence:

$$Re\Big\{\sum_{k=0}^{K-1} C_k^* \sum_{m=0}^{K-1} Y_m e^{-j\epsilon\pi\frac{m^2}{K}} e^{2j\pi\frac{mk}{K}}\Big\} = Re\Big\{\sum_{k=0}^{K-1} C_k^* Z_k^{(\epsilon)}\Big\}$$
$$= \sum_{k=0}^{K-1} |Z_k^{(\epsilon)}|^2 \tag{18}$$

We deduce from (17) that the adapted receiver consists in evaluating $M^{(\epsilon)} = \sum_{k=0}^{K-1} |Z_k^{(\epsilon)}|^2$ for both values of epsilon. The suggested adapted receiver is illustrated in Fig. 5, and summarized in Algorithm 2.

Algorithm 2: Receiver adapted to chirp selection.

input : $Y_0Q_0, .., Y_{K-1}Q_{K-1}$

output: $\hat{\epsilon}, \hat{C}_0^{(\hat{\epsilon})}, .., \hat{C}_{K-1}^{(\hat{\epsilon})}$

$Z_k^{(1)} = IDFT(Y_mQ_me^{-j\pi\frac{m^2}{K}})$

$Z_k^{(-1)} = IDFT(Y_mQ_me^{j\pi\frac{m^2}{K}})$

$M^{(1)} = \sum_{k=0}^{K-1} |Z_k^{(1)}|^2$

$M^{(-1)} = \sum_{k=0}^{K-1} |Z_k^{(-1)}|^2$

if $M^{(1)} > M^{(-1)}$ **then**

  $\hat{\epsilon} = 1$

else

  $\hat{\epsilon} = -1$

$\hat{C}_k = Z_k^{(\hat{\epsilon})}$

V. Generalization to Multi-User OCDM

A. Multi-User OCDM System Model

It can be observed in Fig. 2 that the DFT and the multiplication by the chirp can be seen as a transform precoding leading to pre-coded elements X_m, which are carried by orthogonal subcarriers. Thus, instead of applying a DFT of size K and multiplying by the chirp $e^{j\pi\frac{m^2}{K}}$, it is possible to split the K subcarriers into subsets of subcarriers allocated to different users.

The suggested multi-user OCDM transmitter in illustrated in Fig. 6. We assume that U users can be served by independently pre-coded data streams. Then the K available subcarriers are split into U disjoint subsets composed of $K^{(u)}$ subcarriers such that

$$K = \sum_{u=0}^{U-1} K^{(u)}, \tag{19}$$

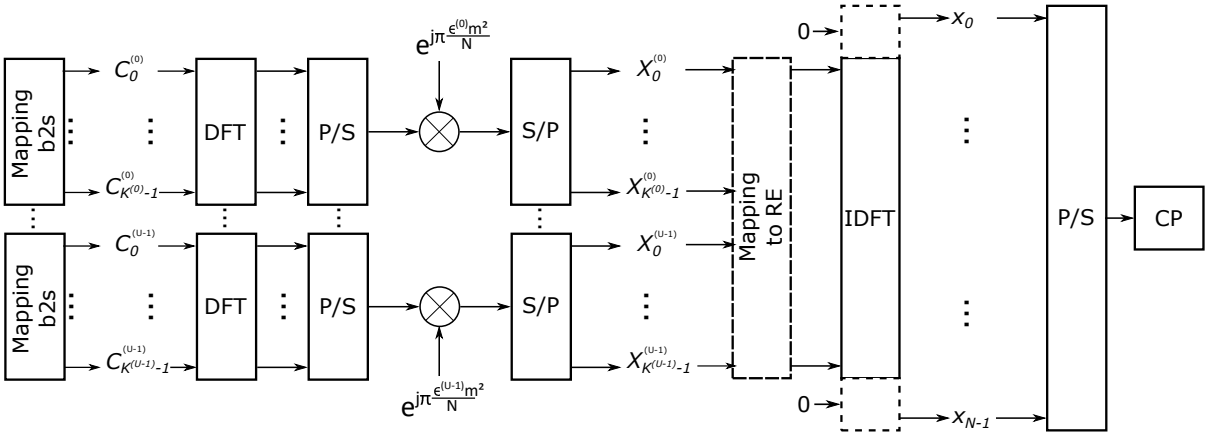

Fig. 6. Multi-user DFT-based OCDM modulation.

where (u) indicates the index of a given user. The simplest solution consists in allocating contiguous subcarriers to each user, but a more general approach could consists in mapping each user stream to a subset of non-contiguous subcarriers, but this is out of the scope of this paper. Then, the U pre-coded data stream $\{X_0^{(u)}, X_1^{(u)}, .., X_{K^{(u)}-1}^{(u)}\}$, $u = 0, 1, .., U-1$ can be possibly mapped to physical resources elements (RE) and modulated through the IDFT (this correspond to the mapping from virtual to physical RE in 5G for instance). The resulting transmitted signal (without specific RE mapping) has the general expression:

$$x_n = \sum_{u=0}^{U-1} \frac{\sqrt{K^{(u)}}}{K^{(u)}N} \sum_{m=0}^{N-1} \alpha_m \underbrace{e^{j\pi \frac{(m-Q^{(u)})^2}{K^{(u)}}} \left[\sum_{k=0}^{K^{(u)}-1} C_k^{(u)} e^{-2j\pi \frac{k(m-Q^{(u)})}{K^{(u)}}} \right]}_{X_m^{(u)}} e^{2j\pi \frac{mn}{N}}, \tag{20}$$

where $Q^{(u)}$ is defined as

$$Q^{(u)} = Q + \sum_{v=0}^{u-1} K^{(v)}, \tag{21}$$

and $\sum_{v=0}^{u-1} K^{(v)} = 0$ for $u = 0$. At the receiver side, each UE applies a DFT of size N, then possibly the inverse mapping from RE, and processes the decoding steps (multiplication by the conjugate chirp and the DFT) over its dedicated K^u subcarriers, such as described in Fig. 2-(b).

B. PAPR Reduction in Multi-User OCDM

The methods OCDM-CS and OCDM-CDCS presented in Section III can be straightforwardly adapted to multi-user OCDM. In fact, the variation of the chirps can be set up or

down in each branch $u = 0, 1, .., U-1$ by setting $\epsilon^{(u)} = \pm 1$, such as illustrated in Fig. 6. Otherwise, it can be noted that the method can be used in a single-user OCDM as well. In that case, the original data stream $\{C_0, C_1, .., C_{K-1}\}$ can be split into U sub-streams transmitted over U sub-bands, each sub-band being pre-coded using upchrips or downchirps. The total number of generated signals is then 2^U, and the transmitter can choose among the signals the one minimizing the PAPR in OCDM-CS or the one minimizing the clipping noise in OCDM-CDCS. As a consequence, the PAPR reduction of the OCDM-CS in multi-user should be improved compared with usual OCDM-CS since the set of signal is larger (2^U against only 2). An adapted receiver including U estimators of $\epsilon^{(u)}$ must be implemented to recover the data. Thus, the complexity of the method grows exponentially with U at the transmitter side, and linearly at the receiver side.

VI. PAPR Performance Analysis

In this section, we analyze the performance of the suggested OCDM-CS in term of PAPR for single-user (with only one band, *i.e.* $U = 1$). To this end, we assume that $x_n^{(1)}$ and $x_n^{(-1)}$ are weakly correlated enough such that the following approximation holds:

$$\begin{aligned}&\mathbb{P}\left(\frac{\max_n |x_n^{(1)}|^2}{\mathbb{E}\{|x_n^{(1)}|^2\}} \geq \lambda, \frac{\max_n |x_n^{(-1)}|^2}{\mathbb{E}\{|x_n^{(-1)}|^2\}} \geq \lambda\right)\\ &\approx \mathbb{P}\left(\frac{\max_n |x_n^{(1)}|^2}{\mathbb{E}\{|x_n^{(1)}|^2\}} \geq \lambda\right)\mathbb{P}\left(\frac{\max_n |x_n^{(-1)}|^2}{\mathbb{E}\{|x_n^{(-1)}|^2\}} \geq \lambda\right).\end{aligned} \tag{22}$$

In fact, we show that the correlation between $x_n^{(1)}$ and $x_n^{(-1)}$ sampled at Nyquist rate and if N is even (typically a power of 2), is given by

$$\left|\frac{\mathbb{E}\{x_n^{(1)}(x_n^{(-1)})^*\}}{\sigma_x^2}\right| = \sqrt{\frac{2}{N}}, \tag{23}$$

which is weak for $N >> 1$, which is generally the case in numerous standards and technologies.

Proof: We use the definition of $x_n^{(1)}$ and $x_n^{(-1)}$ in (9) to obtain

$$\begin{aligned}\mathbb{E}\{x_n^{(1)}(x_n^{(-1)})^*\} =& \frac{e^{j\frac{\pi}{2}}}{N^2}\sum_{k_1=0}^{N-1}\sum_{k_2=0}^{N-1}\mathbb{E}\{C_{k_1}C_{k_2}^*\}\exp\Big(-j\frac{\pi}{N}((n-k_1)^2+(n-k_2)^2)\Big)\\ =& \frac{e^{j\frac{\pi}{2}}}{N^2}\sum_{k=0}^{N-1}\exp\Big(-j\frac{\pi}{N}(2n^2+2k^2-4kn)\Big),\end{aligned} \tag{24}$$

where the cross factors vanish since $\mathbb{E}\{C_{k_1}C_{k_2}^*\} = 0$ when $k_1 \neq k_2$, and $\mathbb{E}\{C_k C_k^*\} = 1$. Then, by using the development of generalized Gaussian sums, we obtain:

$$\begin{aligned}\mathbb{E}\{x_n^{(1)}(x_n^{(-1)})^*\} =& \frac{e^{j\frac{\pi}{2}}e^{-2j\pi\frac{\pi n^2}{N}}}{N^2}\left|\frac{N}{2}\right|^{1/2}\exp\Big(-j\frac{\pi}{8N}(|2N|-16n^2)\Big)\underbrace{\sum_{k=0}^{1}\Big(j\frac{\pi}{2}(N^2+4kn)\Big)}_{=2}\\ =&\sqrt{\frac{2}{N^3}}e^{j\frac{\pi}{4}}. \end{aligned} \tag{25}$$

Moreover, we have $\sigma_x^2 = \mathbb{E}\{x_n^{(1)}(x_n^{(1)})^*\} = \mathbb{E}\{x_n^{(-1)}(x_n^{(-1)})^*\} = \frac{1}{N}$, which concludes the proof.

It results from (22) and (8) that the CCDF of the PAPR of OCDM-CS (highlighted by the superscript CS) is given by

$$\begin{aligned}CCDF^{CS}(\lambda) =& \mathbb{P}\left(\min\Big(\frac{\max_n|x_n^{(1)}|^2}{\mathbb{E}\{|x_n^{(1)}|^2\}}, \frac{\max_n|x_n^{(-1)}|^2}{\mathbb{E}\{|x_n^{(-1)}|^2\}}\Big) \geq \lambda\right)\\ =&\mathbb{P}\left(\frac{\max_n|x_n^{(1)}|^2}{\mathbb{E}\{|x_n^{(1)}|^2\}} \geq \lambda, \frac{\max_n|x_n^{(-1)}|^2}{\mathbb{E}\{|x_n^{(-1)}|^2\}} \geq \lambda\right)\\ =&(1-(1-e^{-\lambda})^N)^2. \end{aligned} \tag{26}$$

Since $CCDF(\lambda) < 1$ ($CCDF$ defined in 8), then we deduce that $CCDF^{CS}(\lambda) < CCDF(\lambda)$, which shows that the suggested technique actually reduces the PAPR of the transmitted signal. Furthermore, similarly to [23], we generalize the result obtained in (26) to oversampled signal as $CCDF^{CS}(\lambda) = (1-(1-e^{-\lambda})^{\alpha N})^2$ with $\alpha = 2.8$. Note that it may be very difficult to generalize this result for multi-user OCDM as the U generated signals are correlated. Nevertheless, it is worth emphasizing that $CCDF^{CS}(\lambda)$ (26) is exactly similar to that obtained using SLM with two phase sequences such as given in [17]. This confirms the aforementioned similarity between OCDM-CS and SLM methods.

VII. Simulations Results

Simulations have been performed with matlab to evaluate the performance of the suggested OCDM-CS and OCDM-CDCS methods in terms of PAPR and BER, as well as the generalization to multi-user OCDM. To this end, signals with $N \in \{256, 512\}$ subcarriers has been used, and the results have been averaged over 20000 simulations runs. Furthermore, a CP of length $N_{CP} = \frac{N}{16}$ has been considered in all simulations.

A. OCDM-CS

In the first series of simulations, random OCDM signals have been generated with N =256 subcarriers and a 16-QAM constellation. Fig. 7 shows the CCDF of PAPR versus the threshold λ (dB) of OFDM and OCDM signals sampled at Nyquist rate (a) and oversampled by a factor 8 (b). We compare the results obtained for OFDM, OCDM, and OCDM-CS. In the latter case, simulations and theoretical performance are plotted. It can be observed in both Figs. 7-(a) and (b) that $CCDF(\lambda)$ of OFDM and OCDM match, since they are both multicarrier waveforms. Moreover, it is shown that a gain is achieved by using the suggested chirp selection method for PAPR reduction, *e.g.* 1.5 dB gain at $CCDF(\lambda) = 10^{-3}$. This proves the relevance of the suggested method, which is not destructive for the signal. It can also be noticed that the theoretical and the simulations results in (26) match, therefore validating the PAPR performance analysis in Section VI. In addition, the analytic performance (26) also holds for SLM method, which can be seen as a benchmark for performance comparison.

We analyze the BER performance versus SNR (dB) in Fig. 8 for coded OFDM, OCDM, and OCDM-CS with the ML adapted receiver. Both AWGN (a) and multipath Rayleigh channel (b) have been considered, where the channel is of length $L = \frac{N_{CP}}{4}$ with an uniform delay profile. A turbo-code similar to the one considered in [33] has been used. Thus, the channel coding has a rate $1/2$, with a random interleaving. In Fig. 8-(a), we observe that the BER performance of OFDM, OCDM, and OCDM-CS is the same, which shows that OFDM and OCDM are equivalent in term of BER in AWGN on one hand, and in the other hand, that the suggested adapted receiver does not induce BER performance loss. In Fig. 8-(b) we observe that OCDM and OCDM-CS outperforms OFDM for $SNR \geq 20$ dB with a gain of 7 dB at BER=0.01, which highlights the capability of coded OCDM to better cope with frequency selectivity than coded OFDM such as highlighted in [3], [4]. On the other hand, we also observe that OCDM and OCDM-CS with the adapted receiver achieve the same BER performance, which, once again, proves that the suggested adapted receiver does not induce BER performance loss, while improving the PAPR.

B. OCDM-CDCS

Fig. 9 shows the CCDF of PAPR versus the threshold λ (dB) for the OCDM without clipping (reference), the clipped OCDM, and the OCDM-CDCS using a 64-QAM constellation, $N = 512$, and $P_t \in \{0.01, 0.001, 0.0001\}$. We do not show the PAPR performance of OFDM to keep the figure clear, but simulations results show that OFDM and OCDM have the same

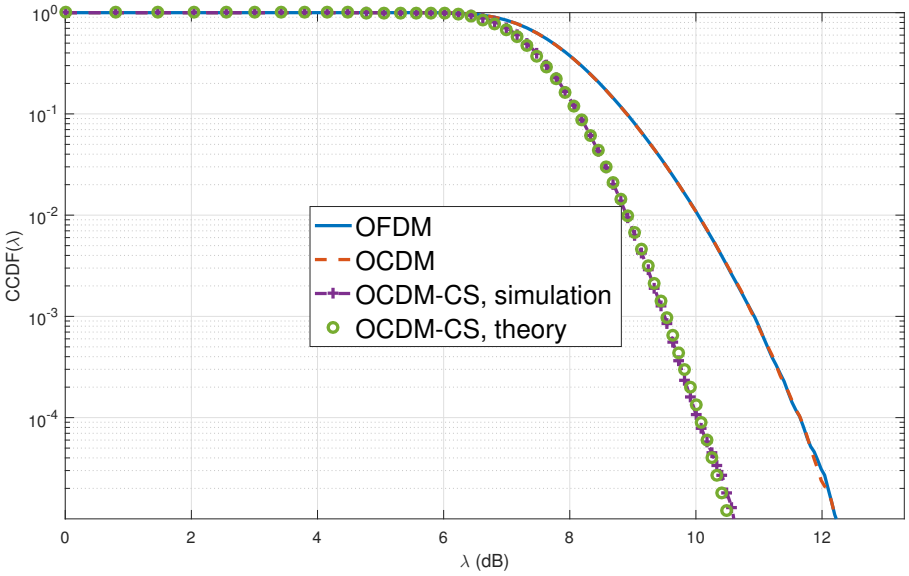

(a) Nyquist rate.

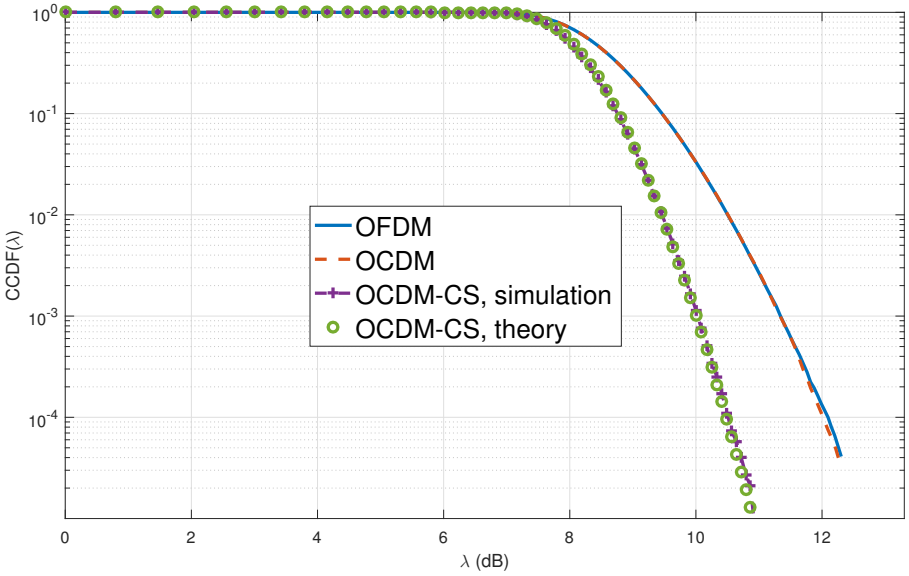

(b) Oversampling rate 8.

Fig. 7. CCDF of PAPR versus threhold λ (dB). Comparison of PAPR performance of OFDM, OCDM, OCDM-CS theorey and simulations, at Nyquist rate (a) and oversampling rate 8 (b).

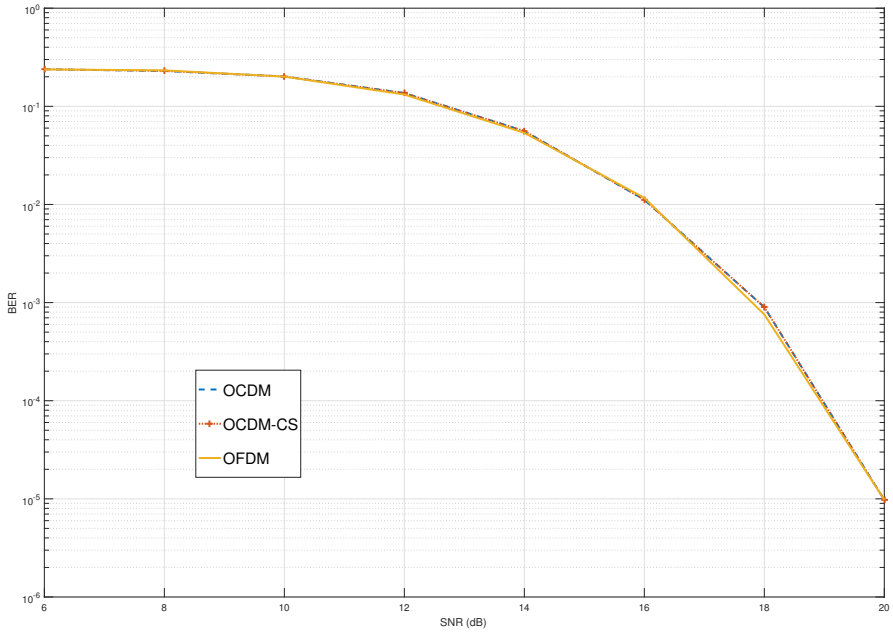

(a) AWGN.

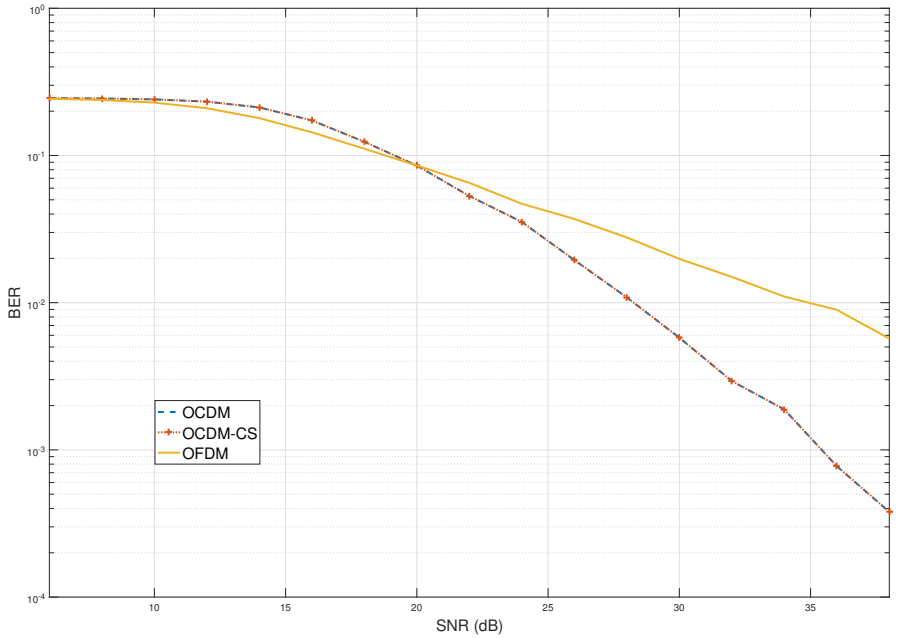

(b) Rayleigh channel.

Fig. 8. BER versus SNR (dB) for coded OFDM, OCDM and OCDM-CS with adapted receiver, and for AWGN (a) and Rayleigh channel (b).

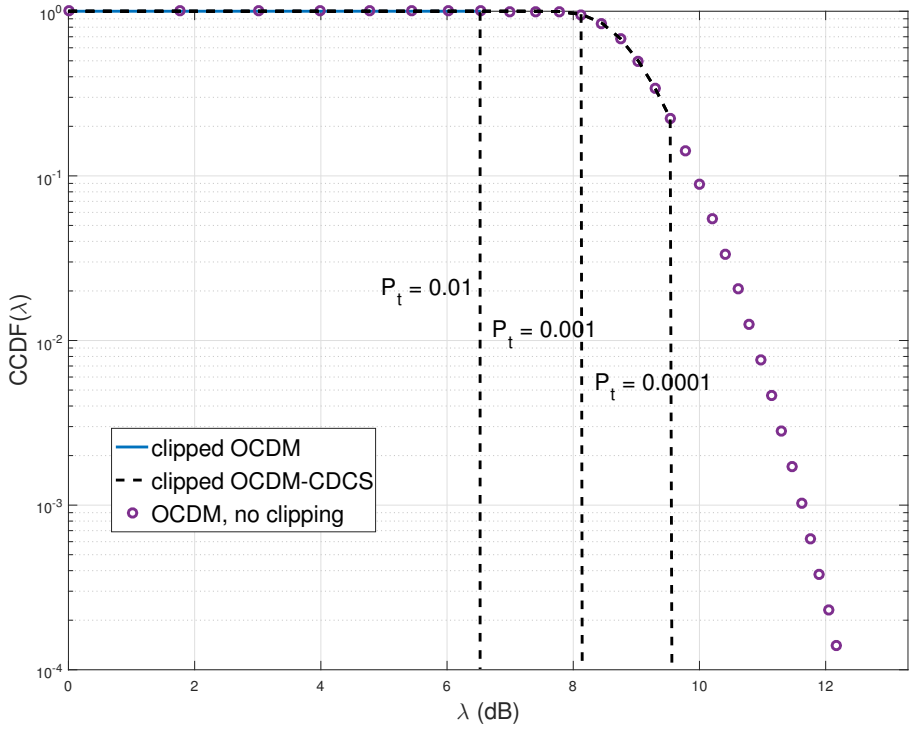

Fig. 9. $CCDF(\lambda)$ versus threshold λ (dB) for OCDM, clipped OCDM, and clipped OCDM-CDCS, and $P_t \in \{0.01, 0.001, 0.0001\}$.

performance, such as observed previously. Moreover, both clipped OCDM and OCDM-CDCS achieve the same PAPR performance as they outperform OCDM without clipping since the PAPR is upper bounded. This result shows that the suggested method allows the transmitter to reach the PAPR performance of usual clipping method, and to perfectly adjust the maximum achievable PAPR by setting P_t.

We plot in Fig. 10 the power spectral density (PSD) (dB) versus normalized frequency (from 0 to 0.5) of OCDM, clipped OCDM, and OCDM-CDCS with $P_t = 0.01$ in order to evaluate the degradation of the out-of-band emission (OOBE) due to the clipping. The signals have been generated with an oversampling rate of 4, and averaged over 1000 independent runs. It can be observed in Fig. 10 that the clipped OCDM and OCDM-CDCS have a slightly higher OOBE compared with OCDM without clipping. In fact the OOBE of the clipped OCDM is locally 5dB higher than that of the OCDM. Furthermore, no noticeable difference can be observed between the clipped OCDM and the OCDM-CDCS method, *i.e.* the latter has no clear advantage compared with the clipped OCDM with respect to the OOBE improvement.

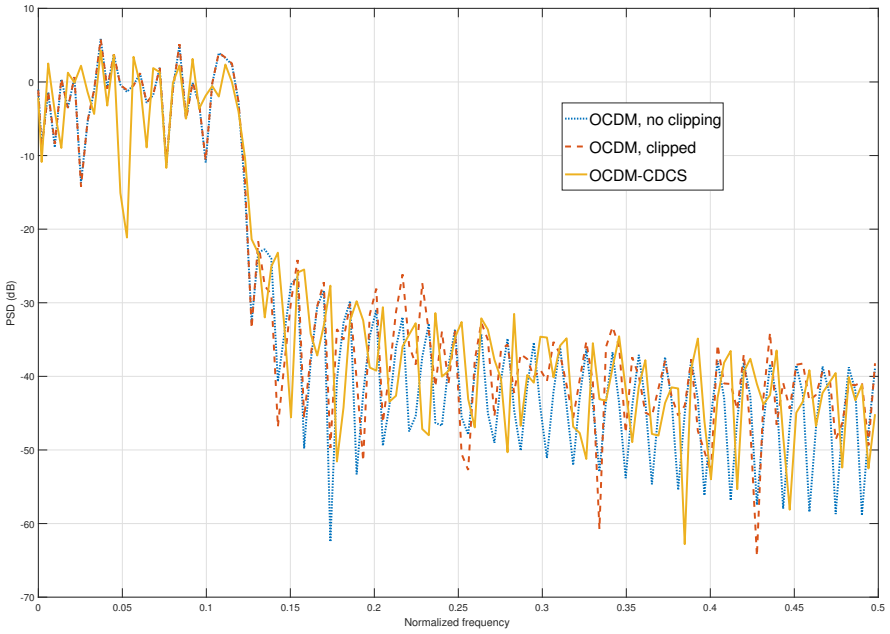

Fig. 10. Power spectral density (PSD) (dB) versus normalized frequency of OCDM, clipped OCDM, and OCDM-CDCS with $P_t = 0.01$.

Figs. 11, 12, and 13 show the BER performance versus SNR (dB) of the non-coded clipped OFDM (referred as OFDM in legend), clipped OCDM (referred as OCDM in legend), and OCDM-CDCS for 16-, 64-, and 256-QAM and 16-, 64-, and 256-PSK constellations, respectively, and using an AWGN channel. In all figures, for any P_t value, and any constellation, we observe that the clipped OFDM and the clipped OCDM reach the same BER performance. Otherwise, Fig. 11 shows that the clipped OCDM-CDCS outperforms the clipped OCDM for $P_t = 0.1$ for both 16-QAM and 16-PSK. This also especially noticeable in Fig. 12 and in Fig. 13 for both $P_t = 0.01$ and $P_t = 0.001$, although it is less noticeable for PSK in the considered SNR range. In fact, we observe that the overall BER performance is better for QAM than PSK, which is consistent with theory. It is especially noticeable that in condition of 256-QAM and $P_t = 0.001$, the BER performance of the clipped-OCDM reaches a lower bound of about 2.10^{-5}, whereas the clipped OCDM-CDCS does not in the considered SNR range. These results shows the capability of the proposed OCDM-CDCS technique to mitigate the clipping noise and therefore improve the BER performance, while ensuring a PAPR as low as expected. Finally, it can be emphasized that similar conclusions can be drawn (OCDM-CDCS

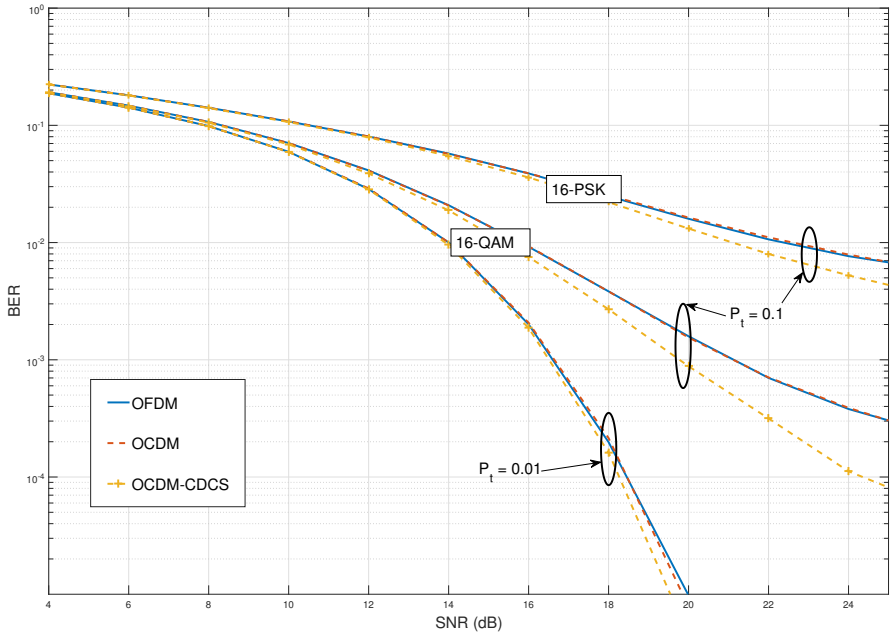

Fig. 11. BER versus SNR (dB) for clipped OFDM, clipped OCDM, and clipped OCDM-CDCS, 16-QAM and 16-PSK constellations and $P_t \in \{0.1, 0.01\}$.

outperforms OCDM with clipping) for coded modulations, but the corresponding figures are not shown in this paper.

C. Multi-User OCDM

Fig. 14 shows the CCDF of PAPR versus the threshold λ (dB) of OCDM, OCDM-CS with 1 band (or equivalently 1 user, *i.e.* $U = 1$), and OCDM-CS with 2 sub-bands (or 2 users, *i.e.* $U = 2$). $N = 256$ subcarriers and a 16-QAM constellation have been used. As expected, the OCDM-CS method using 2 sub-bands achieves a lower PAPR than that of the OCDM-CS with only one band. In fact, a gain of 3 dB (resp. 1 dB) is achieved by the OCDM-CS with 2 sub-bands compared with OCDM (resp. OCDM-CS with one band), for $CCDF(\lambda) = 10^{-4}$. This shows the capability of OCDM-CS to largely reduce the PAPR without any signal distortion, loss of data rate, and loss of performance.

VIII. Conclusion

In this paper, we have presented two PAPR reduction methods for OCDM systems. Both techniques are based on the selection of the frequency variations of the chirps at the trans-

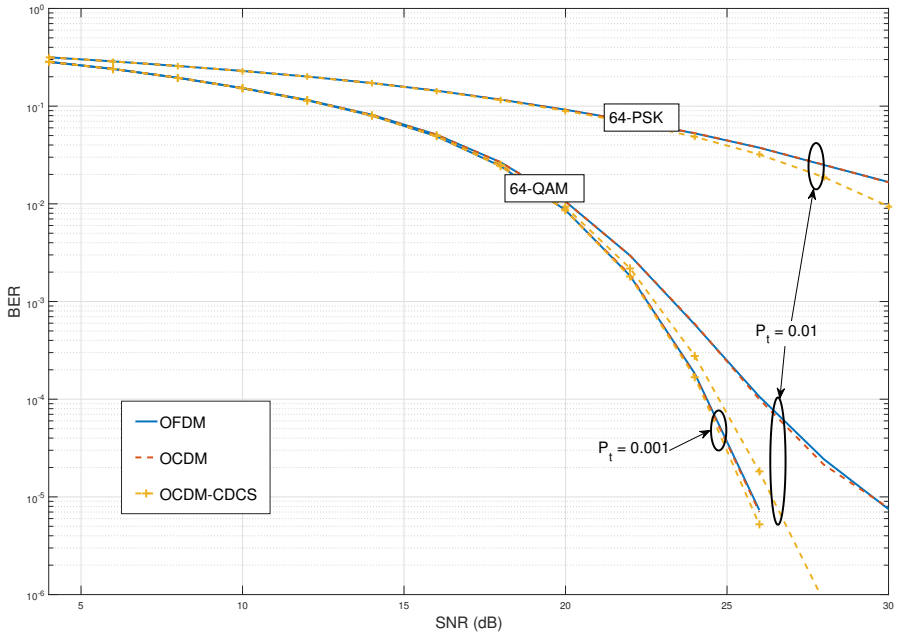

Fig. 12. BER versus SNR (dB) for clipped OFDM, clipped OCDM, and clipped OCDM-CDCS, 64-QAM and 64-PSK constellations and $P_t \in \{0.01, 0.001\}$.

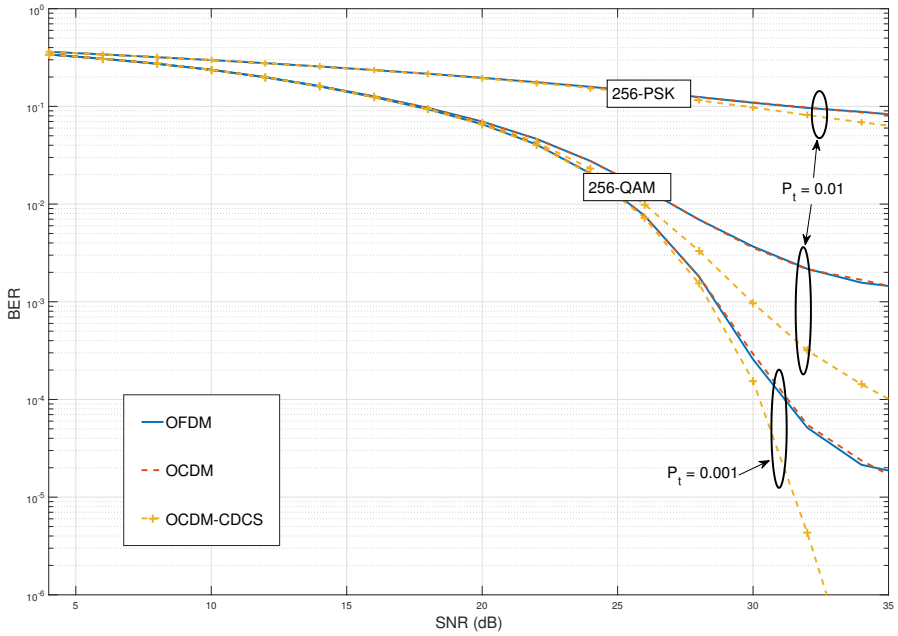

Fig. 13. BER versus SNR (dB) for clipped OFDM, clipped OCDM, and clipped OCDM-CDCS, 256-QAM and 256-PSK constellations and $P_t \in \{0.01, 0.001\}$.

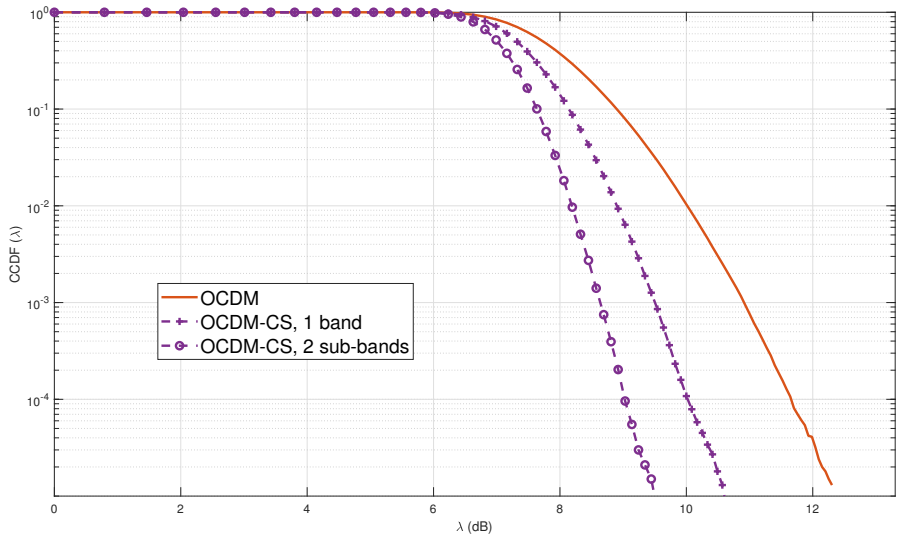

Fig. 14. $CCDF(\lambda)$ versus threshold λ for OCDM, OCDM-CS with 1 band (1 user), and OCDM-CS with 2 sub-bands (or 2 users).

mitter. The first method, called OCDM-CS, selects one of the generated signal (with up or down chirps) according to the minimum achieved PAPR. In the second one called OCDM-CDCS, both signals are clipped, and the one featuring the lowest clipping noise is selected to be transmitted. Both methods are original and dedicated to OCDM, as they are based on chirp selection. Furthermore, we have presented the multi-user OCDM system, in which the K subcarriers can be split into subsets that can be allocated to different users. Then, the suggested PAPR reduction principles have been generalized to this multi-user OCDM system model. Simulations results show that the OCDM-CS actually reduces the PAPR of the signal without BER performance loss. The OCDM-CDCS, in turn, drastically reduces the PAPR thanks to the clipping, with a limited BER performance loss by reducing the clipping noise. Future works will be undertaken to evaluate the effect of channel estimation instead of perfect estimation on the suggested method.

REFERENCES

[1] X. Ouyang and J. Zhao, "Orthogonal Chirp Division Multiplexing," *IEEE Transactions on Communications*, vol. 64, no. 9, pp. 3946–3957, 2016.

[2] 3GPP, "3GPP TS 38.211, Physical channels and modulation (Release 16, v16.2.0)," 3GPP, Tech. Rep., July 2020.

[3] R. Bomfin, M. Chafii, and G. Fettweis, "Low-Complexity Iterative Receiver for Orthogonal Chirp Division Multiplexing," in *2019 IEEE Wireless Communications and Networking Conference Workshop (WCNCW)*, 2019, pp. 1–6.

[4] R. Bomfin, D. Zhang, M. Matthé, and G. Fettweis, "A Theoretical Framework for Optimizing Multicarrier Systems Under Time and/or Frequency-Selective Channels," *IEEE Communications Letters*, vol. 22, no. 11, pp. 2394–2397, 2018.

[5] Q. Wang, A. Kakkavas, X. Gong, and R. A. Stirling-Gallacher, "Towards Integrated Sensing and Communications for 6G," in *2022 2nd IEEE International Symposium on Joint Communications & Sensing (JC&S)*, New-York, USA, March 2022, pp. 1–6.

[6] J. R. Klauder, A. C. Price, S. Darlington, and W. J. Albersheim, "The theory and design of chirp radars," *The Bell System Technical Journal*, vol. 39, no. 4, pp. 745–808, 1960.

[7] V. Savaux, "Flexible Communication System for 6G Based on Orthogonal Chirp Division Multiplexing," in *1st IEEE 6G Networking Conference (6GNet)*, Paris, France, july 2022.

[8] M. S. Omar and X. Ma, "Spectrum Design for Orthogonal Chirp Division Multiplexing Transmissions," *IEEE Wireless Communications Letters*, vol. 9, no. 11, pp. 1990–1994, 2020.

[9] R. Hadani, S. Rakib, M. Tsatsanis, A. Monk, A. J. Goldsmith, A. F. Molisch, and R. Calderbank, "Orthogonal Time Frequency Space Modulation," in *2017 IEEE Wireless Communications and Networking Conference (WCNC)*, 2017, pp. 1–6.

[10] A. Bemani, N. Ksairi, and M. Kountouris, "AFDM: A Full Diversity Next Generation Waveform for High Mobility Communications," in *2021 IEEE International Conference on Communications Workshops (ICC Workshops)*, 2021, pp. 1–6.

[11] A. Bemani, G. Cuozzo, N. Ksairi, and M. Kountouris, "Affine frequency division multiplexing for next-generation wireless networks," in *2021 17th International Symposium on Wireless Communication Systems (ISWCS)*, Berlin, Germany, September 2021, pp. 1–6.

[12] X. Ouyang, G. Talli, M. Power, and P. Townsend, "Orthogonal chirp-division multiplexing for IM/DD-based short-reach systems," *Opt. Express*, vol. 27, no. 16, pp. 23 620–23 632, Aug 2019. [Online]. Available: http://opg.optica.org/oe/abstract.cfm?URI=oe-27-16-23620

[13] Z. Hu, X. Ouyang, J. Zhao, P. Townsend, and C.-K. Chan, "Investigation of a Low-Complexity Transceiver for Orthogonal Chirp Division Multiplexing based IM/DD OWC Systems," in *2019 24th OptoElectronics and Communications Conference (OECC) and 2019 International Conference on Photonics in Switching and Computing (PSC)*, Fukuoka, Japan, July 2019, pp. 1–3.

[14] Y. Bai and P.-J. Bouvet, "Orthogonal Chirp Division Multiplexing for Underwater Acoustic Communication," *Sensors*, vol. 18, no. 11, 2018. [Online]. Available: https://www.mdpi.com/1424-8220/18/11/3815

[15] P. Zhu, X. Xu, X. Tu, Y. Chen, and Y. Tao, "Anti-Multipath Orthogonal Chirp Division Multiplexing for Underwater Acoustic Communication," *IEEE Access*, vol. 8, pp. 13 305–13 314, july 2020.

[16] R. Bomfin, M. Chafii, and G. Fettweis, "Performance Assessment of Orthogonal Chirp Division Multiplexing in MIMO Space Time Coding," in *2019 IEEE 2nd 5G World Forum (5GWF)*, Dresden, Germany, November 2019, pp. 220–225.

[17] H. Attar, "Peak-to-Average Power Ratio Performance Analysis for Orthogonal Chirp Division Multiplexing Multicarrier Systems Based on Discrete Fractional Cosine Transform," *International Journal of Communications, Network and System Sciences*, vol. 2016, no. 9, pp. 545 – 562, 2016.

[18] X. Lv, J. Wang, Z. Jiang, and W. Jiao, "A novel PAPR reduction method for OCDM-based radar-communication signal," in *2018 IEEE MTT-S International Microwave Workshop Series on 5G Hardware and System Technologies (IMWS-5G)*, 2018, pp. 1–3.

[19] M. S. Omar and X. Ma, "Pilot symbol aided channel estimation for ocdm transmissions," *IEEE Communications Letters*, vol. 26, no. 1, pp. 163–166, 2022.

[20] V. Savaux and P. Savelli, “Frequency domain preamble-based channel estimation and equalization in LoRa,” *International Journal of Mobile Network Design and Innovation*, vol. 10, no. 2, pp. 74 – 81, 2021.

[21] B. C. Berndt, R. J. Evans, and K. S. Williams, *Gauss and Jacobi Sums*. Ney York: John Wiley and Sons, 1996, ch. 1: Gauss Sums, pp. 7 – 56.

[22] X. Ouyang and J. Zhao, “Orthogonal Chirp Division Multiplexing for Coherent Optical Fiber Communications,” *Journal of Lightwave Technology*, vol. 34, no. 18, pp. 4376 – 4386, 2016.

[23] R. Van Nee and A. De Wild, “Reducing the peak-to-average power ratio of OFDM,” in *proc. of VTC’98*, Ottawa, Ont., Canada, May 1998.

[24] H. Ochiai and H. Imai, “On the Distribution of the Peak to Average Power Ratio in OFDM Signals,” *IEEE Transactions on Communications*, vol. 49, no. 2, pp. 282 – 289, February 2001.

[25] V. Savaux and Y. Louët, “PAPR Analysis as a Ratio of Two Random Variables: Application to Multicarrier Systems With Low Subcarriers Number,” *IEEE Transactions on Communications*, vol. 66, no. 11, pp. 5732 – 5739, 2018.

[26] A. Frömming, L. Häring, and A. Czylwik, “Spectral Properties of Clipping Noise,” *Mathematics*, vol. 9, no. 20, 2021. [Online]. Available: https://www.mdpi.com/2227-7390/9/20/2592

[27] S. Thompson, J. Proakis, and J. Zeidler, “The effectiveness of signal clipping for PAPR and total degradation reduction in OFDM systems,” in *GLOBECOM ’05. IEEE Global Telecommunications Conference, 2005.*, vol. 5, 2005, pp. 5 pp.–2811.

[28] C. Browning, D. Dass, P. Townsend, and X. Ouyang, “Orthogonal chirp-division multiplexing for future converged optical/millimeter-wave radio access networks,” *IEEE Access*, vol. 10, pp. 3571–3579, 2022.

[29] X. Ouyang, C. Antony, G. Talli, and P. D. Townsend, “Robust Channel Estimation for Coherent Optical Orthogonal Chirp-Division Multiplexing With Pulse Compression and Noise Rejection,” *Journal of Lightwave Technology*, vol. 36, no. 23, pp. 5600–5610, 2018.

[30] S. Bhattacharjee, K. V. Mishra, R. Annavajjala, and C. R. Murthy, “Evaluation of Orthogonal Chirp Division Multiplexing for Automotive Integrated Sensing and Communications,” in *ICASSP 2022 - 2022 IEEE International Conference on Acoustics, Speech and Signal Processing (ICASSP)*, 2022, pp. 8742–8746.

[31] M. L. de Filomeno, L. G. de Oliveira, A. Camponogara, A. Diewald, T. Zwick, M. L. R. de Campos, and M. V. Ribeiro, “Joint Channel Estimation and Schmidl & Cox Synchronization for OCDM-Based Systems,” *IEEE Communications Letters*, vol. 26, no. 8, pp. 1878–1882, 2022.

[32] R. Zhang, Y. Wang, and X. Ma, “Channel Estimation for OCDM Transmissions With Carrier Frequency Offset,” *IEEE Wireless Communications Letters*, vol. 11, no. 3, pp. 483–487, 2022.

[33] H. Ochiai and H. Imai, “Performance analysis of deliberately clipped OFDM signals,” *IEEE Transactions on Communications*, vol. 50, no. 1, pp. 89–101, 2002.